SolarPACES 2024, 30th International Conference on Concentrating Solar Power, Thermal, and Chemical Energy Systems

Thermal Energy Storage Materials, Media, and Systems

https://doi.org/10.52825/solarpaces.v3i.2350

Published: 25 Nov. 2025

Evaluation of Alternative Base Materials for Mitigation of Stress Relaxation Cracking in Thermal Energy Storage Tanks

Timothy Pickle[1], Joel Harvey[1], Theodore Vassi[2], Ravi Vishnu[2], Paul Janiak[2], Andy Backhouse[2], Sergio Davila[3], Bruce Leslie[4], Kurt Drewes[4], and Zhenzhen Yu[1,5,*]

[1]Colorado School of Mines, Golden, Colorado, USA

[2]Outokumpu Stainless AB, Avesta, Sweden

[3]Contratos y Diseños (CYD) Industriales, Barcelona, Spain

[4]Vast, Darlinghurst, Australia

[5]National Renewable Energy Laboratory, Golden, Colorado, USA

*Correspondence: Zhenzhen Yu, zyu@mines.edu

Abstract. Concentrating solar power plants with thermal energy storage face challenges related to stress relaxation cracking (SRC) in molten hot salt tanks. While alloy 347H stainless steel is commonly employed due to its stress corrosion cracking (SCC) resistance and sufficient mechanical properties, it suffers from SRC in the weld region. This study explores alloy 1.4910 as a potential alternative, known for its superior creep strength and molten salt corrosion resistance. Thermomechanical testing using a Gleeble® 3500 physical simulator reveals promising results for alloy 1.4910 heat affected zone (HAZ) and 16-8-2 filler (ER16.8.2) fusion zone (FZ), with no cracking observed within a 22-hour test period at elevated temperatures ranging from 600 to 800°C and initial true stress conditions of 650 MPa (0.174 strain) for HAZ and 460 MPa (yield strength) for FZ. In contrast, alloy 347H HAZ and matching filler FZ experienced cracking within a few hours at 800°C. Metallurgical characterization and fractography are additionally conducted on cross welded 1.4910 samples with 16-8-2 filler and thermomechanical Gleeble® samples.

Keywords: Molten Salt Storage Tank, Stress Relaxation Cracking, Welding, Stainless Steel

1. Introduction

Thermal energy storage systems employing molten hot salt tanks in concentrating solar power plants face challenges related to weld performance cracking, particularly in alloy 347H austenitic stainless steel [1-3]. This stainless-steel grade possesses enhanced stress corrosion cracking (SCC) resistance and elevated temperature mechanical strength in comparison to 304H and 316H grades [4]. However, intergranular stress relaxation cracking (SRC) could emerge months to years in service in 347H stainless-steel weldments due to the presence of weld-induced residual stresses and susceptible microstructures under elevated service temperature of 565°C. While post weld heat treatment may alleviate cracking by stress relief and stabilizing the microstructure, implementation of post weld heat treatment in the field can be challenging and could potentially contribute to higher temperature SRC during the process if not carefully

designed [5, 6]. Additionally, various industries, including concentrating solar power, have looked at 316H stainless-steel as a potential alloy, but the nuclear industry in the past decades have reported hundreds of SRC failures in advanced gas cooled reactors using 316H stainless-steel [7, 8], and in general, 316H stainless-steel is argued to have high susceptibility to SRC based on various industry failures and lab scale testing results [9, 10].

To mitigate SRC concerns, there is an increasing demand in evaluating alternative alloys and weld fillers with improved SRC resistance and comparable thermomechanical properties (e.g., creep and fatigue) and corrosion resistance. Alloy 1.4910, an alternative alloy to 316H known as 316LNB (low carbon and added nitrogen and boron content), with good creep resistance [11] and comparable or similar molten salt corrosion resistance compared to 347H [12, 13]. A study on a similar grade, 347 AP (low carbon and high nitrogen variation of 347H), demonstrated improved SRC resistance on a lab scale [14]. Additionally, the use of 16-8-2 filler has been demonstrated to improve toughness and thermomechanical properties as an alternative filler to matching fillers in 347H and 304H SS welds [15]. The purpose of this work is to evaluate the SRC resistance of alloy 1.4910 and its weld using 16-8-2 filler, specifically using a Gleeble® thermomechanical testing procedure, in comparison to 347H SS welds, as a potential alternative candidate material for concentrating solar power hot salt tank application.

2. Experimental Procedures

2.1 Material and Welding Experiments

Table 1 summarizes the chemical compositions of the two alloys of interest, 1.4910 and 347H stainless-steel. Alloy 1.4910, e.g., 316LNB, is a low carbon alloy with higher concentrations of molybdenum, nickel, nitrogen, and boron and no Nb with respect to alloy 347H. The weld filler chosen for alloy 1.4910 is ER16.8.2, a solid wire used for gas tungsten arc welding. The matching filler for 347H SS is E347-16, shielded metal arc welding electrode and filler.

Table 1. *Alloying chemical composition (in wt.%) of heats studied of alloy 1.4910 and 347H, respectively, and weld fillers ER16.8.2 and E347-16.*

Alloy/Filler	1.4910	347H	ER16.8.2	E347-16
C	0.013	0.05	0.051	0.03
Si	0.38	0.51	0.48	0.54
Mn	1.06	1.0	1.35	1.5
Cr	17.06	17.3	15.0	19.5
Ni	12.05	9.1	8.6	10.1
Nb	-	0.58	0.01	0.36
Mo	2.54	0.32	1.22	0.2
Cu	-	0.21	0.09	0.16
Ti	-	-	0.002	-
V	-	-	0.03	-
S	0.001	0.002	0.002	0.01
P	0.026	0.029	0.013	0.02
N	0.155	0.03	0.04	0.03
B	0.003	-	-	-

Alloy 1.4910 was welded using ER16.8.2 filler and gas tungsten arc welding process on 20 mm thick plates. The joint geometry is a single-V groove with a 60° total groove angle and a 5-mm wide root gap with no root landing. A backing bar with 3 mm thickness and 20 mm width was implemented for the duration of welding, and it was removed after completion of multi-pass welding. Figure 1(c) shows the joint geometry of the weld. The weld current was about 110-120 amperage, the voltage was 11-13 volts, and the travel speed was 10-15 cm per

minute. The weld arc energy per unit length was maintained less than 0.94 kJ/mm per weld pass.

2.2 Thermomechanical Testing

A Gleeble® 3500 thermomechanical physical simulator is used to study SRC in welded microstructures using a four-step methodology as seen in Figure 1, including testing of physically simulated 1.4910 heat-affected zone (HAZ) and extracted cross-welded 16-8-2 fusion zone (FZ) samples. For HAZ microstructural duplication, firstly, a thermal cycle is applied using Gleeble® machine using a profile extracted from finite element simulation of welding process [16]. Peak temperatures of 1332 and 1277°C were initially selected for the thermal cycle in step 1 (see Figure 1(a)). Since a couple of samples partially melted on heating to 1332°C peak temperature, all further testing was then carried out with the peak temperature of 1277°C. Analysis of the 1332°C peak temperature HAZ microstructure is ongoing. Secondly, as seen in Figure 1(b), a stress representing residual stress conditions (~450-600 MPa) is applied at room temperature. Thirdly, samples are heated to a target testing temperature between 600 and 800°C along with an applied additional stroke to compensate for thermal expansion. At last, when reaching test temperature, the displacement becomes constrained, and samples are held at temperature up to 22 hours. If samples do not fail within 22 hours, they are pulled to failure to measure strain to failure. More information on this procedure can be seen elsewhere [5, 17]. All samples, including HAZ and extracted weld FZ samples, were machined using uniaxial sub size ASTM E8 specification [18], as seen in Figure 1 (d).

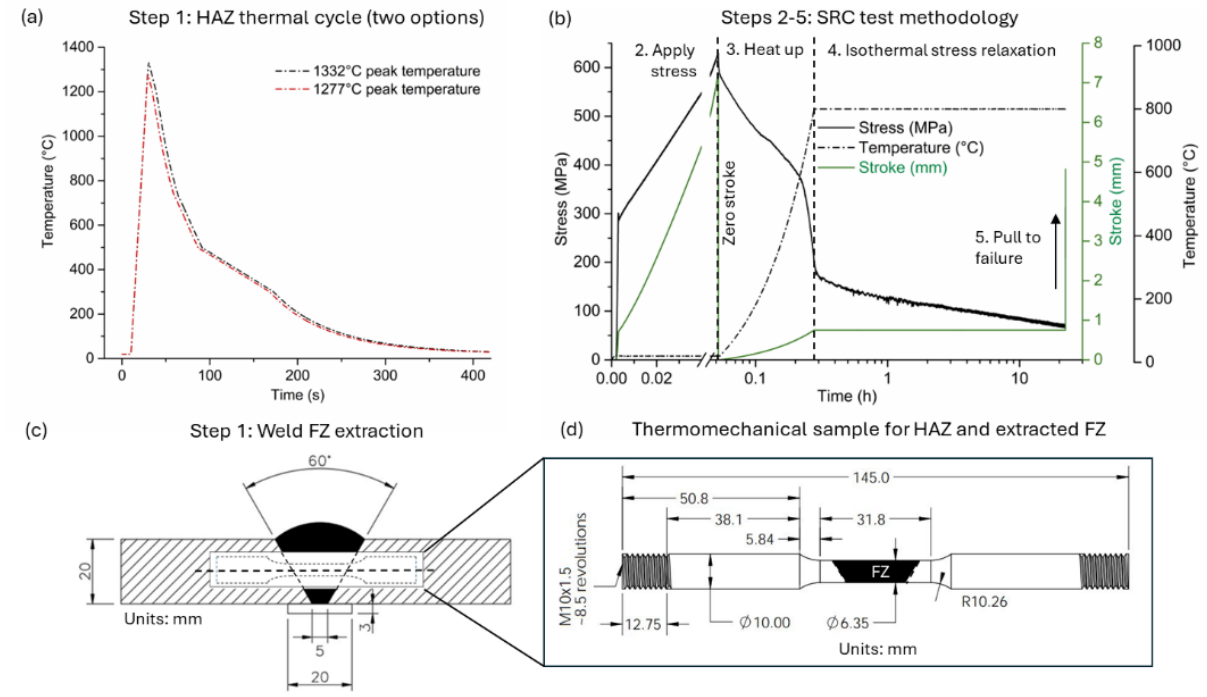

Figure 1. *Gleeble® SRC methodology (a) step 1 single pass HAZ physical simulation performed on a wrought specimen, (b) four-step SRC test methodology of both HAZ or weld FZ, (c) weld FZ sample extraction with respect to weld joint (step 1 for weld FZ), and (d) specific thermomechanical sample geometry dimensions (using ASTM E8 sub-size round samples [18]) for both HAZ and extracted weld FZ.*

2.3 Metallurgical Characterizations

Metallurgical characterization, using light optical microscopy (LOM), was conducted to evaluate etched (electrolytic etch using 2V and 200 mA parameters and 40% diluted nitric acid)

microstructure of weld specimens and physically simulated Gleeble® HAZ samples. Vicker's microhardness mapping, using 500 g load, was additionally conducted on weld specimens, including in 16-8-2 FZ, 1.4910 HAZ, and the partially melted zone (PMZ) regions. Fractography analysis using LOM was also briefly performed on SRC test specimens. Thermodynamic calculations were conducted to predict equilibrium and non-equilibrium solidification phases.

3. Results and Discussion

3.1 Weld Microstructures

The weld microstructure and microhardness in the as-welded condition for weld and as-received condition are shown in Figure 2. The LOM images on the FZ boundary etches darker than the centre of FZ and in the HAZ, indicating the presence of a PMZ. Microhardness maps were taken of the weld joint FZ and further out into the base metal (BM). The FZ boundary, or PMZ, and HAZ adjacent to PMZ contains higher microhardness peaks above 250 HV compared to most of the weld FZ and BM, which is mostly 170-180 HV in mid-thickness. Strain hardening from welding, formation of precipitates, or both strengthening mechanisms could contribute to this localized hardening along the FZ boundary. Microhardness approaches 200 HV close to the surface of the 20 mm thick plate in the unaffected 1.4910 BM. Highest microhardness regions, particularly exceeding 250 HV, have been correlated with higher susceptibility to SRC compared to softer regions [19].

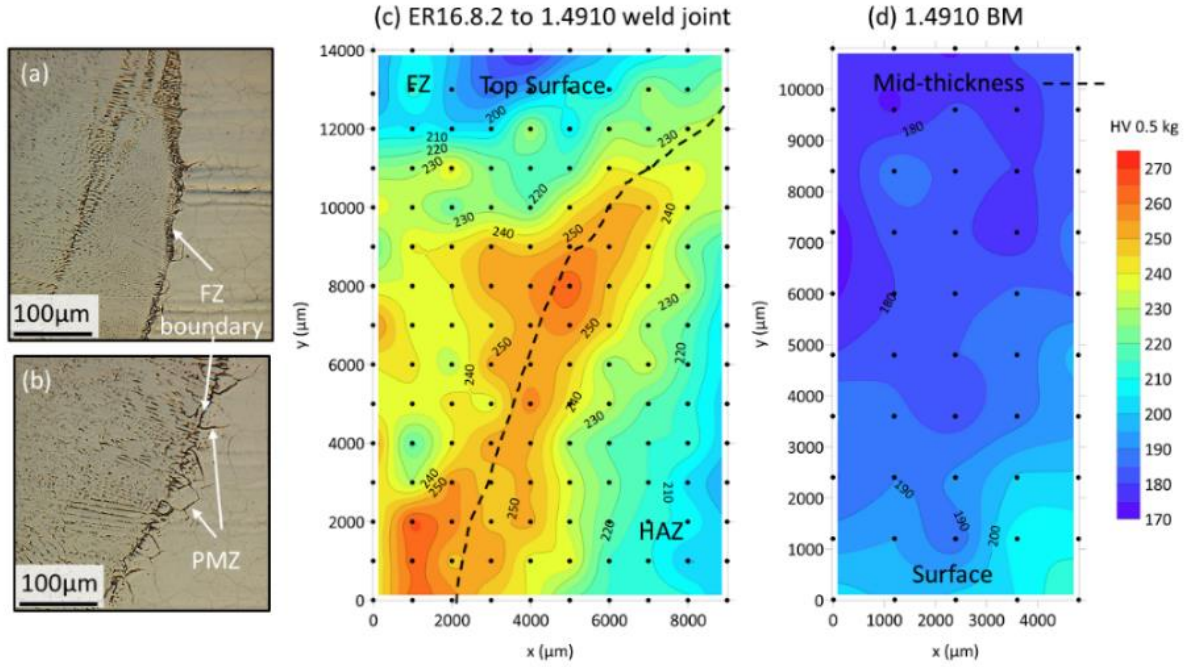

Figure 2. *(a-b) ER16.8.2-1.4910 GTA weld microstructure using LOM, (c) Vicker's microhardness map of weld FZ and HAZ centered on FZ boundary, and (d) relative Vicker's microhardness map of unaffected base metal.*

Thermodynamic simulations were conducted using Thermocalc® software to predict the equilibrium microstructure of alloy 1.4910 and ER16.8.2 undiluted filler. Figure 3 shows the single-axis equilibrium volume fraction of phases as a function of temperature and Scheil diagrams predicting non-equilibrium solidification phases, primarily δ-ferrite followed by austenite (ferrite-to-austenite solidification mode). The higher temperature phases will be more kinetically favourable to form during welding and processing of plate material. For instance, slow cooling rates during welding may help facilitate the precipitation of M_3B_2 particles, rich in Mo,

in HAZ while FZ may develop $M_{23}C_6$ precipitates. Additionally, M_2B type borides has been seen with a 310LNB type SS [20]. Other low temperature phases, such as η-intermetallic [21], sigma or α-ferrite particularly in 16-8-2 [22], may develop after thousands of hours at temperature.

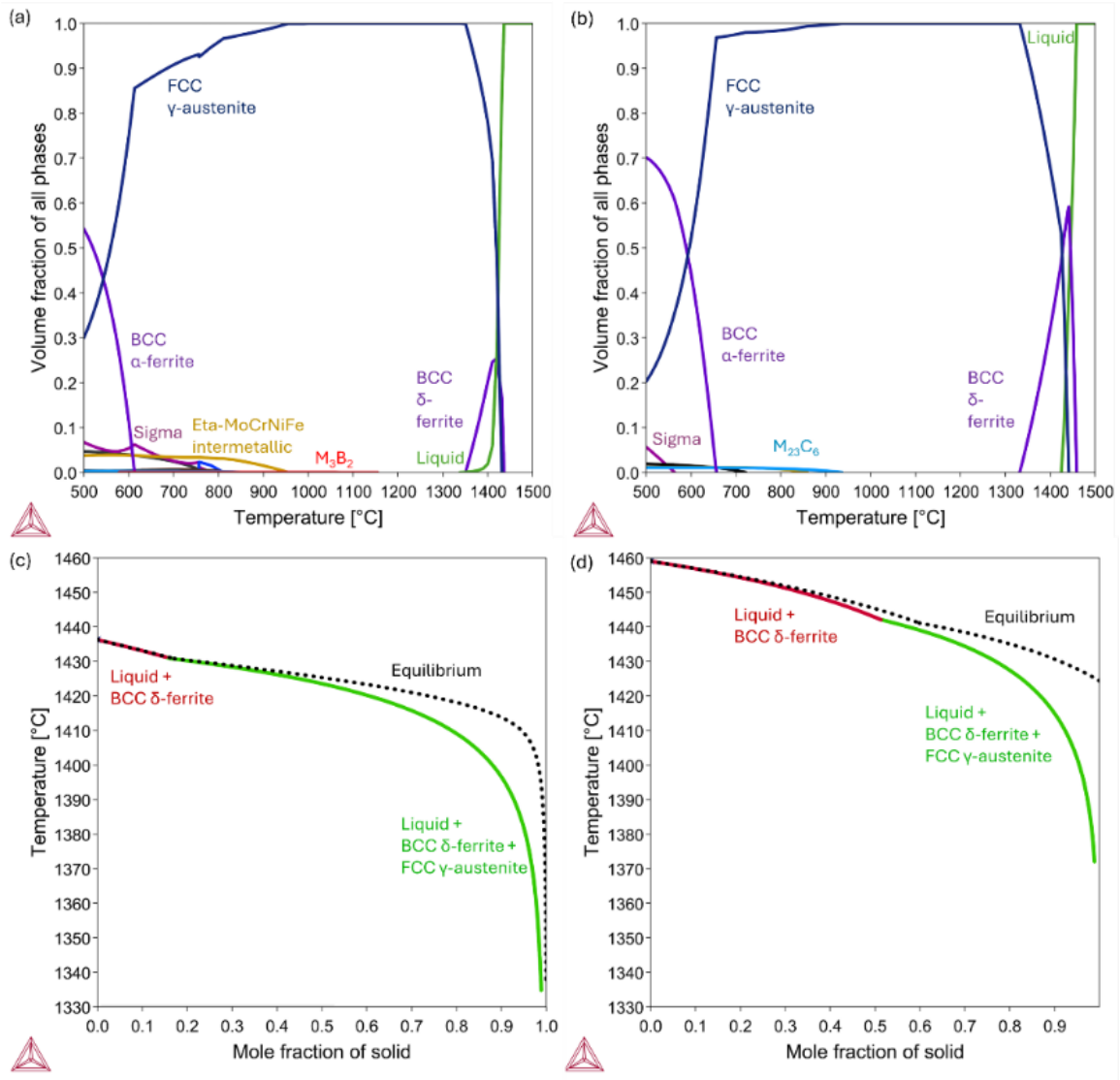

Figure 3. *CALPHAD equilibrium single-axis phase diagram using (a) alloy 1.4910 BM composition and (b) ER16.8.2 composition (undiluted) and Scheil diagram of (c) 1.4910 and (d) ER16.8.2.*

3.2 SRC test results of alloy 1.4910 and 347H SS

The main thermomechanical test results are summarised in Table 2 from 1.4910 HAZ and ER16.8.2 FZ. Overall, none of the samples failed during the SRC tests. More information for the specific tests is further provided.

The thermomechanical test results of the ER16.8.2 FZ for three temperature conditions of 600, 700, and 800°C are shown in Figure 4. From the stress relaxation profile in Figure 4 (a), the samples did not fail within a 22-hour time at temperature. The diametral strain at center gauge section increases with test temperature shown in Figure 4 (b), which likely indicates more creep strain as reported in another publication on similar test method [17]. However, none of them cracked under stress relaxation conditions. After the 22-hour hold time, samples are pulled to failure using a strain rate (10^{-3}/s) and are illustrated in load-displacement in Figure

4 (c). The 800°C test condition exhibited the least ductility during the final step and may be due to more creep strain accumulation during stress relaxation.

Table 2. *Experimental test results using Gleeble®3500 thermomechanical physical simulator. ROA-reduction of area (NOTE: ROA accounts for initial and final diameters-initial ROA of HAZ during step 2 is 17%).*

Material	**Sample**	**Peak HAZ temp. (°C)**	**Initial RT stress range (MPa) /strain (step 2)**	**Start-ing stress at step 4 temp. (MPa)**	**Step 4 temp. (°C)**	**Step 4 time (h)**	**SRC re-sult**	**Step 5b strain to peak load/peak stress (MPa)/ ROA (%)**
ER16.8.2 FZ	W1	N/A	470	149	800	22	No fai-lure	0.08/204/43
	W3		457	250	700	22	No fai-lure	0.15/385/77
	W4		448	286	600	22	No fai-lure	0.06/390/78
1.4910 simula-ted HAZ	H1	1332	628-586/0.174	202	800	22	No fai-lure	0.14/332/76
	H4	1277	639-597/0.174	201	800	22	No fai-lure	0.12/310/85
	H5	1277	651-610/0.174	206	800	22	No fai-lure	0.12/345/85
	H6	1277	677-630/0.174	333	700	22	No fai-lure	0.12/452/83
	H7	1277	678-632/0.174	393	600	22	No fai-lure	0.06/506/76

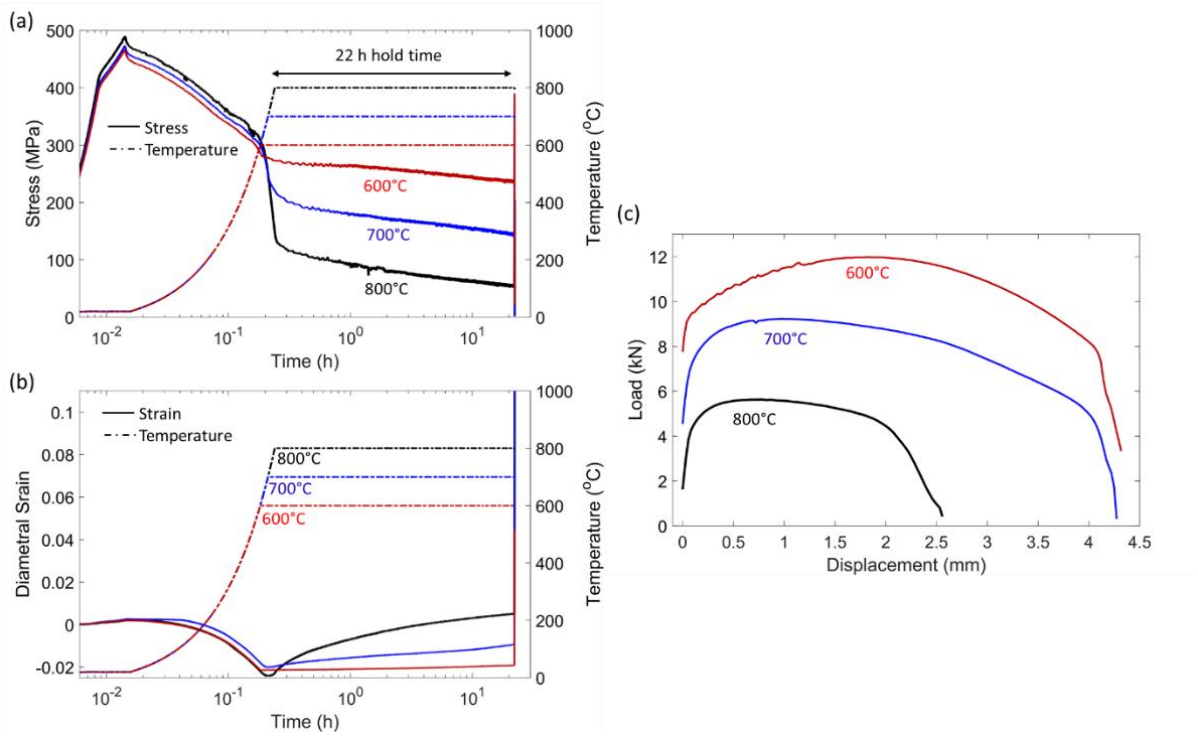

Figure 4. *Thermomechanical test data of ER16.8.2 FZ (a) stress as a function of temperature and time, (b) diametral strain as a function of temperature and strain, (c) load-displacement during step five after stress relaxation.*

Figure 5 shows the thermomechanical test data for alloy 1.4910 at 600, 700, and 800°C. There was no failure occurring during stress relaxation within a 22-hour time for all three temperature conditions. While there was no cracking during stress relaxation, more creep strain developed at 800°C, as expected, than 700°C or 600°C. Additionally, the sample tested at 800°C with a higher peak temperature HAZ thermal cycle from step one (1332°C) seemed to incur more creep strain than the HAZ with a lower peak temperature of 1277°C, as seen with grey line compared to black lines in Figure 5 (b). While no failure happened during stress relaxation, the load-displacement curves indicate lower ductility and no post uniform elongation at 600°C, which is different than observed with the ER16.8.2 FZ. Further work may be needed to analyse the susceptibility of alloy 1.4910 HAZ to SRC at 600°C for longer time periods.

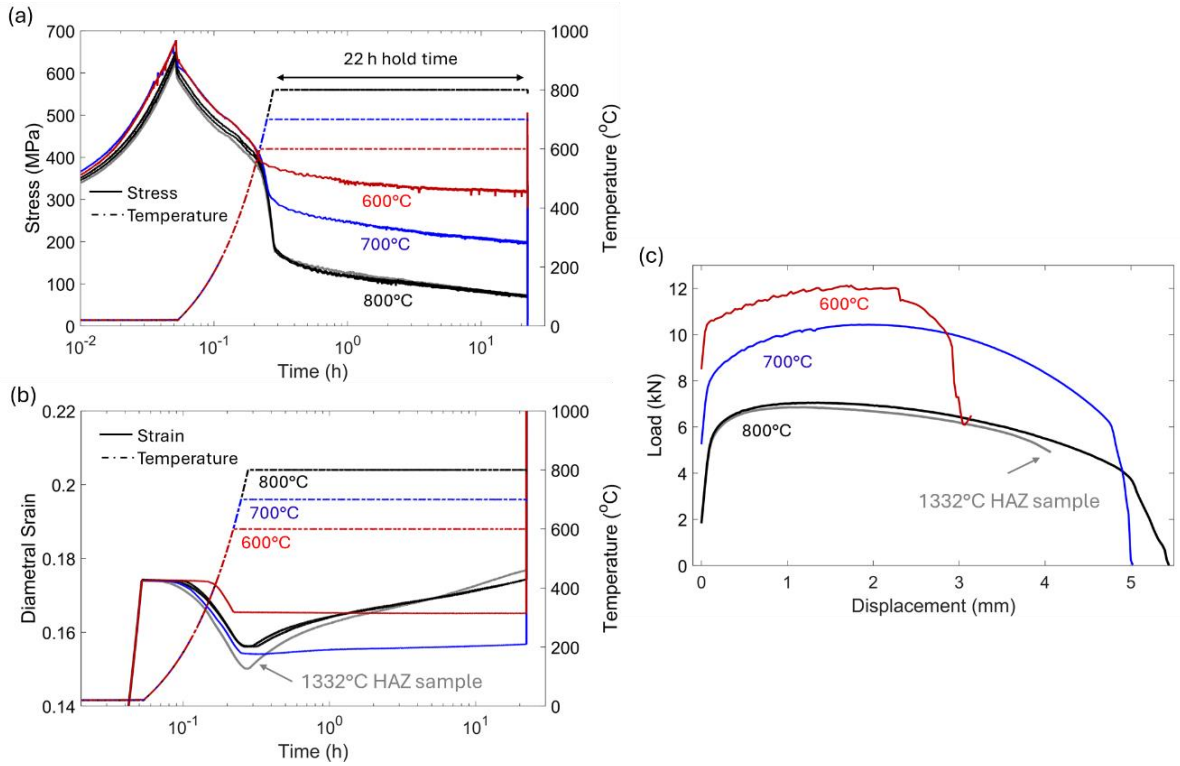

Figure 5. *Thermomechanical test data of alloy 1.4910 HAZ (a) stress as a function of temperature and time, (b) diametral strain as a function of temperature and strain, (c) load-displacement during step five after stress relaxation.*

Characterization of the fracture surfaces and cross-sections near the fracture surface and bulk of a few HAZ samples are shown in Figure 6. Significant grain deformation behind the fracture surface and transgranular fracture can be observed on LOM images behind fracture surface. Additionally, the effect of the HAZ higher peak temperature (1332°C) on the microstructure can be seen with a darker etching response in a non-necked region using LOM, as seen in Figure 6 (c) in comparison to (f). It is worth noting the lower post-uniform ductility and reduction of area during the step five pull-to-failure of the 1332°C peak temperature HAZ, as seen in Figure 5 (c), may be explained by the presence of secondary phases reducing post uniform ductility. Similar dark etching features in Figure 6 (f) were seen along the FZ boundary in Figure 2 (a-b). Further analysis is needed to verify the presence of secondary phase in this sample as well as in the weld and determine whether borides or boronitrides are present. The effect of the HAZ thermal cycle and specific location in HAZ may influence microstructure susceptibility with respect to SRC, and authors will further analyze this effect.

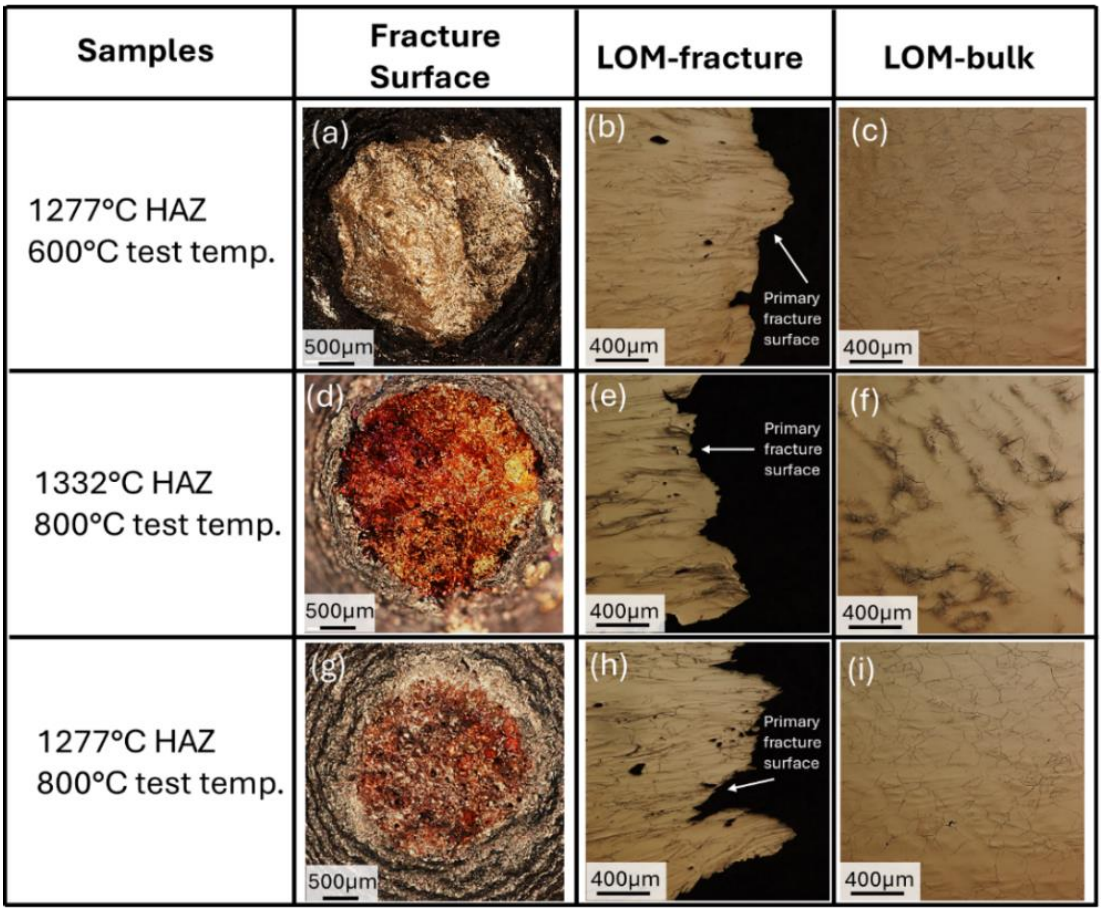

Figure 6. *Fractographic and LOM analysis near fracture surfaces and bulk after thermomechanical testing of (a-c) sample #7 (1277°C HAZ; 600°C test temperature), (d-f) sample #1 (1332°C HAZ; 800°C test temperature, (g-i) sample #4 (1277°C HAZ; 800°C test temperature).*

3.3 Comparison of SRC between alloy 4910 and 347H SS HAZ and weld filler FZ of ER16.8.2 and E347-16

Similar SRC studies on 347H SS and their welds have been published by the same authors elsewhere, including the HAZ and extracted FZ samples from welds using matching E347 filler [5, 17]. As a first step comparison of SRC susceptibility, alloy 1.4910 and 347H SS HAZs using 1332-1335°C peak temperature is compared in Figure 7 (a-b). With the same applied HAZ thermal cycle and stress and strain, 347H SS HAZ fails at temperature at about three hours while the 1.4910 alloy does not fail. The creep strain that accumulates during isothermal hold is demonstrably higher in alloy 1.4910 than 347H SS, indicating higher creep resistance in 347H SS. However, SRC preferentially develops in 347H HAZ than 1.4910 HAZ using these lab tests. A comparison of SRC susceptibility at 700 and 800°C between E347 and ER16.8.2 FZ can be seen in Figure 7 (c-d). While the E347 FZ failed quickly at 800°C, it did not fail under stress relaxation within a 24-hour period at 700°C. However, the diametral strain required for fracture upon pulling to failure after the 24-hour period was less than 0.01, indicating lower thermomechanical ductility compared to ER16.8.2 FZ, which was 0.15. None of the ER16.8.2 FZ samples failed under stress relaxation and exhibit better resistance to SRC than E347 FZ at 700 and 800°C.

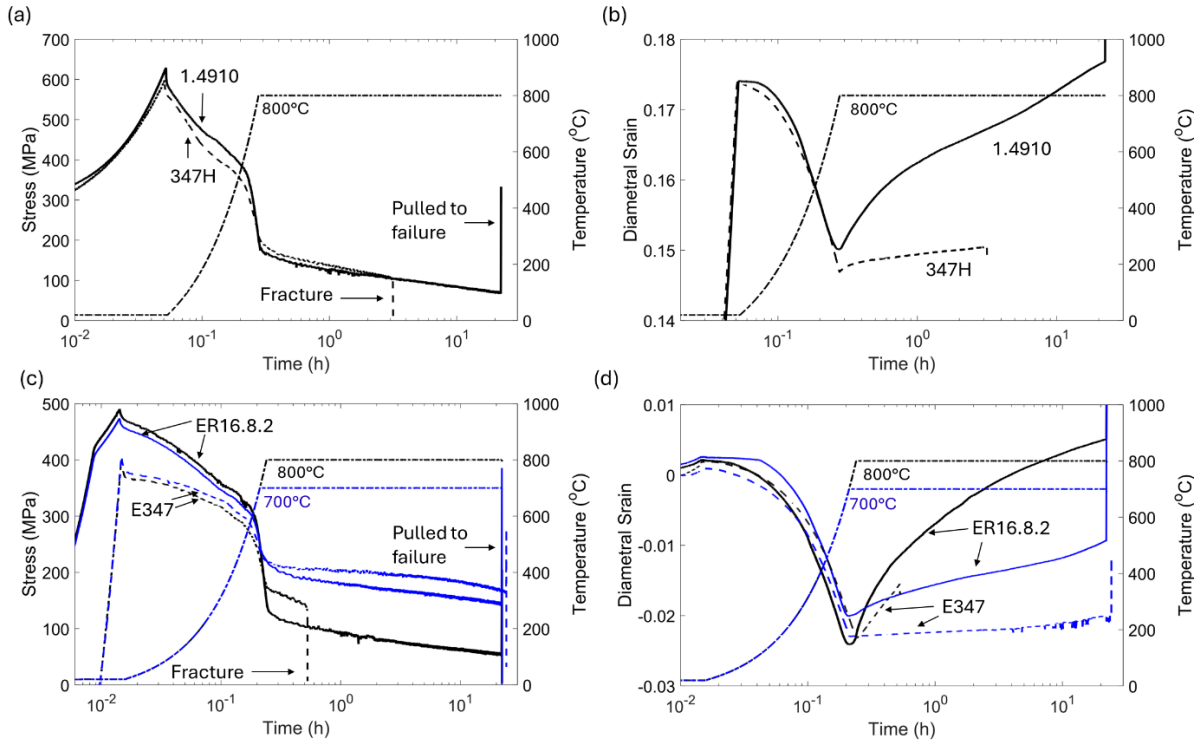

Figure 7. *SRC comparison between (a-b) 347H and 1.4910 HAZ and (c-d) ER16.8.2 and E347 FZ.*

4. Conclusion

Alternative materials, such as alloy 1.4910, provide the potential of replacing commonly used 347H SS that are susceptible to SRC. Alloy 1.4910 was evaluated for SRC susceptibility using a four-step thermomechanical test lab methodology with a Gleeble®3500. The weld HAZ and weld filler FZ, using ER16.8.2, were studied and these results were compared to 347H SS HAZ and matching filler (E347-16) FZ.

The SRC testing results show no cracking for the 22-hour time duration for both 1.4910 HAZ and 16-8-2 FZ, while for alloy 347H HAZ and matching filler E347 FZ samples tested using the same methodology, SRC is observed. For instance, at 800°C, the HAZ and matching filler FZ of alloy 347H failed within three hours at temperature. Hence, the HAZ of alloy 1.4910 and 16-8-2 FZ at the testing conditions used in this study exhibits better resistance to SRC than HAZ of alloy 347H and matching filler FZ. High microhardness regions on FZ boundary and PMZ of alloy 1.4910 may be a localized region with higher SRC susceptibility based on literature studies and could explain why higher peak temperature HAZ region (1332°C) exhibits less thermomechanical ductility than the lower peak temperature (1277°C) HAZ. Future efforts by the authors will focus on completing test matrix (e.g., longer times at 600°C) and investigating microstructural conditions needed for fracture, such as secondary phases in PMZ.

Data availability statement

The original data from experiments are presented in this article. Data from experiments in this study is not publicly available, but further inquiries can be directed to the corresponding author.

Underlying and related material

No underlying or related material is available.

Author contributions

Timothy Pickle-conceptualization, data curation, formal analysis, investigation, methodology, visualization, writing (original draft); Joel Harvey-investigation, methodology; Theodore Vassi-conceptualization, investigation, writing (review & editing); Ravi Vishnu-conceptualization, investigation, writing (review & editing); Paul Janiak-investigation, project administration, resources, supervision, writing (review & editing); Andy Backhouse-investigation, project administration, resources, supervision, writing (review & editing); Sergio Davila-investigation, resources, writing (review & editing); Bruce Leslie-investigation, supervision, writing (review & editing); Kurt Drewes-investigation, project administration, supervision, writing (review & editing); Zhenzhen Yu-conceptualization, investigation, funding acquisition, resources, supervision, visualization, writing (review & editing)

Competing interests

The authors declare that they have no competing interests.

Funding

Work has been funded by Outokumpu Stainless AB and Vast for experimentation and writing preparation of this manuscript.

Acknowledgement

Thanks to Outokumpu Stainless AB for providing alloy 1.4910 steel plate material and to Contratos Y Diseños Industriales SA for welding and machining of test samples.

References

[1] J. D. Osorio, M. Mehos, L. Imponenti, B. Kelly, H. Price, J. Torres-Madronero, et al., "Failure Analysis for Molten Salt Thermal Energy Storage Tanks for In-Service CSP Plants," National Renewable Energy Laboratory (NREL), United States, 2024.
[2] T. Pickle, C. Augustine, and Z. Yu, "Mechanical Failure Risk Management for In-Service CSP Nitrate Hot Tanks," National Renewable Energy Laboratory (NREL), United States, 2024.
[3] C. Augustine, T. Pickle, Y. Hong, J. Vidal, and Z. Yu, "Stress Relaxation Cracking of Alloys at Temperatures Higher Than 540°C," National Renewable Energy Laboratory (NREL), United States, 2024.
[4] R. D. Thomas, Jr. and R. W. Messler, "Welding Type 347 Stainless Steel-An Interpretive Report," Welding Research Council Bulletin, vol. Bulletin 421, 1997.
[5] T. Pickle, Y. Hong, J. Vidal, C. Augustine, and Z. Yu, "Stress relaxation cracking susceptibility evaluation in 347H stainless steel welds," Welding in the World, 2024.
[6] J. C. Lippold and D. J. Kotecki, "Ch. 6 Austenitic Stainless Steel," in Welding Metallurgy and Weldability of Stainless Steels, ed: John Wiley and Sons, Inc., 2005.
[7] J.-W. Rensman, M. W. Spindler, and C. Shargay, "Stress Relaxation Cracking, A Misunderstood Problem in the Process Industry," in ASME 2023 Pressure Vessels & Piping Conference, 2023.
[8] P. Neumann, D. A. Miller, and R. A. Ainsworth, "Material factors which influence remaining life of components subject to reheat cracking," in Fracture, Plastic Flow, and Structural Integrity, ed: CRC Press, 2019, pp. 175-184.
[9] J. C. van Wortel, "Prevention of Relaxation Cracking by Material Selection and or Heat Treatment: Final Report," TNO Institute of Industrial Technology2000.

[10] H. van Wortel, "Control of Relaxation Cracking in Austenitic High Temperature Components," presented at the NACE Corrosion, Nashville, TN, 2007.
[11] T. E. Standard, "EN 10028-7:2016 Flat products made of steels for pressure purposes-Part 7: Stainless Steels," ed.
[12] B. Helmersson, M. Navas, A. Martinez-Tarifa, R. Wu, and A. Backhouse, "Molten Nitrate Corrosion Testing and Creep Data for Stainless Steels," presented at the SolarPACES 2019, Daegu, South Korea, 2020.
[13] A. Bonk, W. Ding, A. Hanke, M. Braun, J. Müller, S. Klein, et al., "Effect of gas management on corrosion resistance in molten solar salt up to 620 °C: Corrosion of SS316-types and SS347," Corrosion Science, vol. 227, p. 111700, 2024.
[14] T. Osuki, Y. Suzuki, S. Kurihara, T. Ono, and M. Ueyema, "Proposal of 18Cr-8Ni based Austenitic Stainless Steel with Superior Stress Relaxation Cracking Resistance," in Association for Materials Production and Performance (AMPP), San Antonio, TX, 2022.
[15] C. Fink, H. Wang, B. T. Alexandrov, and J. Penso, "Filler Metal 16-8-2 for Structural Welds on 304H and 347H Stainless Steels for High Temperature Service," Welding Journal, vol. 99, pp. 312-322, 2020.
[16] Y. U. Hong, T. Pickle, J. Vidal, C. Augustine, and Z. Yu, "Impact of Plate Thickness and Joint Geometry on Residual Stresses in 347H Stainless Steel Welds," Welding Journal, vol. 102, pp. 279-292, 2023.
[17] T. Pickle, Y. Hong, C. Augustine, J. Vidal, and Z. Yu, "Stress Relaxation Cracking in 347H Stainless Steel Arc Welds: Susceptibility Evaluation of Heat-Affected Zone," Metals, vol. 14, p. 494, 2024.
[18] ASTM, "ASTM E8 / E8M - 21 Standard Test Methods for Tension Testing of Metallic Materials," 2021.
[19] R. Kant and J. N. DuPont, "Stress Relief Cracking Susceptibility in High-Temperature Alloys," Welding Journal, vol. 98, pp. 29-49, 2019.
[20] T. Sourmail, T. Okuda, and J. E. Taylor, "Formation of chromium borides in quenched modified 310 austenitic stainless steel," Scripta Materialia, vol. 50, pp. 1271-1276, 2004.
[21] P. J. Maziasz, "The formation of diamond-cubic eta phase in type 316 stainless steel exposed to thermal aging or irradiation environments " Scripta Metallurgica, vol. 13, pp. 621-626, 1979.
[22] O. DeNonno, J. F. Gonzales, S. Tate, R. Hamlin, and J. Klemm-Toole, "Role of Austenite Stability in Elevated Temperature Mechanical Properties of Gas Metal Arc-Directed Energy Deposition Austenitic Stainless Steels," JOM, 2024.